Periodic orbit basis for the quantum baker map

Leonardo Ermann[1,2,]* and Marcos Saraceno[1,3]

[1]*Departamento de Física, Comisión Nacional de Energía Atómica, Avenida del Libertador 8250, C1429BNP Buenos Aires, Argentina*
[2]*Departamento de Física, FCEyN, UBA, Pabellón 1 Ciudad Universitaria, C1428EGA Buenos Aires, Argentina*
[3]*Escuela de Ciencia y Tecnología, Universidad Nacional de San Martín, Alem 3901, B1653HIM Villa Ballester, Argentina*

A set of quantum states, dynamically related to the classical periodic orbits of a chaotic map, is used as a basis in which the description of the eigenstates of its quantum version is greatly simplified. This set can be improved with the inclusion of short time propagation along the stable and unstable manifolds of the periodic orbits resulting in a construction similar to the scar functions of Vergini [J. Phys. A **33**, 4709 (2000)]. The average participation ratio is used to quantify the quality of the basis.

I. INTRODUCTION

The question of the structure of the eigenfunctions of chaotic systems is intimately related to the construction of the bases in which they can be expanded. In this respect a good basis is one in which most eigenstates are given in terms of a limited number of significant coefficients: A good measure being, i.e., the average participation ratio in the given basis. In the generic case of a basis unrelated to the Hamiltonian (or the map) the states are mostly random and the average participation ratio ($\langle PR \rangle$) takes the random matrix value $D/2$ (for a Hilbert space of dimension D). At the other trivial extreme the eigen basis gives a $\langle PR \rangle$ of unity. It is then clear that a "good" basis must incorporate some dynamical elements from the system and at the same time be sufficiently simple so as to be effectively constructed without resorting to a full diagonalization.

In the case of the quantum baker's map (QBM) Lakshminarayan found that the eigenfunctions had a simple structure (and significantly small participation ratio) when looked upon in the Hadamard basis [1], thus exploiting a very special property of the QBM. This line of research was followed in [2], where it was found that the eigenfunctions of a large family of quantizations of the QBM could be described in terms of a very simple map, the essential baker, which for special values of the Hilbert space dimension becomes the Walsh quantized baker and can be explicitly constructed. These features are very special and intimately related to the binary symbolic dynamics of the map and are not easily generalized to other systems.

A different approach with a potentially more general applicability, is based on the construction of states that "live" on the unstable periodic orbits of the system. When used as a basis these states realize in quantum mechanics the ideal of Poincaré in the sense that "they (the periodic orbits) are the only breach through we might try to penetrate into a stronghold hitherto reputed unassailable" [3]. The fact that some eigenstates of chaotic systems show "scars" of periodic orbits was established long ago by Heller [4], in counterpart to earlier works in which the assumption was a uniform distri-

bution on the energy shell according to the microcanonical ensemble [5,6]. The scarring phenomena was studied in several chaotic systems, in which linear and nonlinear theories were developed [7–13].

The construction of scar functions in the QBM is based on early studies in the stadium billiard [10,11,14]. The QBM can be thought of as a pedagogical system to apply these techniques since it has symbolic dynamics, stable (unstable) manifold parallel to q (p) direction, a finite spectrum, and the same small-valued Lyapunov exponent in the entire phase space.

In this paper we provide a recipe to construct a set of scar functions as an accurate basis to describe the QBM. This basis has the propagation time of the quantum propagator as parameter. When this time is of the order of the Heisenberg time, the basis converges to the eigenbase of the map. For short times, of the order of the Ehrenfest time, the basis describes the spectrum of the QBM better than other known bases [1,2].

In Sec. II, we briefly introduce the classical and quantum version of the baker map. We construct the periodic orbit modes and scar functions based on the evolution of the coherent states under the QBM. We give the rule with which we choose a basis to describe the spectrum of the QBM for any even-dimensional Hilbert space in Sec. III. Then, in Sec. IV, we numerically test the basis, computing the average participation ratio as a function of the propagation time. In Sec. V we propose a method to approximate the scar functions by homoclinic periodic orbit modes avoiding evolution in time, and finally, we state the conclusions.

II. CLASSICAL AND QUANTUM EVOLUTION

A. Baker's transformation

In this section we review some properties and notation of the classical baker's map that we will use in the quantum states construction. The baker's map $\mathcal{B}$ [15] is defined in the unit square phase space ($q, p \in [0, 1)$) as

$$q' = 2q - \lfloor 2q \rfloor,$$

$$p' = \frac{(p + \lfloor 2q \rfloor)}{2}, \tag{1}$$

————
*ermann@tandar.cnea.gov.ar

036221-1

where $\lfloor x \rfloor$ is the integer part of x. This map is area-preserving, uniformly hyperbolic with Lyapunov exponent ($\lambda = \ln 2$), and has stable foliation $\{q = \text{cst}\}$ and unstable foliation $\{p = \text{cst}\}$.

The baker map has a simple action upon symbols in the binary expansion of the coordinates

$$(p|q) = \cdots \epsilon_{-1} \cdot \epsilon_0 \epsilon_1 \cdots \xrightarrow{\mathcal{B}} (p'|q') = \cdots \epsilon_{-1} \epsilon_0 \cdot \epsilon_1 \cdots, \quad (2)$$

where $q = \sum_{i=0}^{\infty} \epsilon_i 2^{-(i+1)}$ and $p = \sum_{i=-1}^{-\infty} \epsilon_i 2^i$.

The map has two symmetries:

(i) Parity (R): represented with the exchanges $q \to 1-q$ and $p \to 1-p$ together with the bitwise logical NOT upon symbols ($0 \leftrightarrows 1$).

(ii) Time reversal (T): represented with the exchange $p \leftrightarrows q$ together with reversing the direction of the symbolic flow.

The periodic orbits of the baker map of period L can be represented by binary strings $\boldsymbol{\nu}$ of length L. We denote the different trajectory points on a periodic orbit by (q_j, p_j) for $j = 0, \ldots, L-1$ with $(q_L, p_L) \equiv (q_0, p_0)$. The coordinates of the first trajectory point on the periodic orbit can be obtained explicitly in terms of the binary string

$$q_0 = \boldsymbol{\nu}\boldsymbol{\nu}\boldsymbol{\nu}\cdots = \frac{\nu}{2^L - 1}, \quad (3)$$

$$p_0 = \boldsymbol{\nu}^\dagger\boldsymbol{\nu}^\dagger\boldsymbol{\nu}^\dagger\cdots = \frac{\nu^\dagger}{2^L - 1}, \quad (4)$$

where ν is the integer value of the string $\boldsymbol{\nu}$ which represents a binary number, and $\nu^\dagger$ is the string formed by all L bits of $\boldsymbol{\nu}$ in reverse order. The other trajectory points can be easily calculated by iterations of the map or by cyclic shifts of $\boldsymbol{\nu}$.

B. Quantum baker map

The quantization of the map is performed in an even D-dimensional Hilbert space with $D = 1/(2\pi\hbar)$. The QBM is defined in terms of the discrete Fourier transform with antisymmetric boundary conditions as [16–18]

$$\hat{B} = \hat{G}_D^\dagger \begin{pmatrix} \hat{G}_{D/2} & 0 \\ 0 & \hat{G}_{D/2} \end{pmatrix}, \quad (5)$$

$$\langle j | \hat{G}_D | k \rangle = \frac{1}{\sqrt{D}} \exp\left[-i \frac{2\pi}{D}\left(j + \frac{1}{2}\right)\left(k + \frac{1}{2}\right) \right]. \quad (6)$$

The quantum baker map has the same symmetries as its classical counterpart

$$[\hat{B}, \hat{R}] = 0, \quad (7)$$

$$(\hat{G}\hat{B}\hat{G}^{-1})^* = \hat{B}^{-1} \quad (8)$$

with parity represented by $\hat{R} = -\hat{G}^2$ and time reversal by $\hat{T} = \hat{K}\hat{G}$, where $\hat{K}$ is the complex conjugation operator.

The QBM spectrum is characterized by D eigenphases and eigenstates $\hat{B}|\psi_j\rangle = e^{i\varphi_j}|\psi_j\rangle$, with definite $\hat{R}$ symmetry

($\hat{R}|\psi_j\rangle = \pm|\psi_j\rangle$), and satisfying the time reversal requirement $\hat{G}|\psi_i\rangle = |\psi_i\rangle^*$.

III. BASIS CONSTRUCTION

A. Periodic orbit modes

The first step in our construction is the definition of the periodic orbit modes (POM), a superposition of coherent states centered on the periodic points of an orbit. Similar constructions have been employed before [7–11,19]. Our definition is equivalent to the discrete-time version of the tube functions defined by Vergini and Carlo in [10,11] for continuous Hamiltonian flows.

The coherent state on the D-dimensional Hilbert space on the torus with antiperiodic boundary conditions centered on (q, p) [20] are represented in coordinate basis $|j\rangle$ as

$$\langle j | q, p \rangle = K \sum_{m=-\infty}^{\infty} e^{-\pi D(e_j + m - q)^2} e^{i 2\pi D(e_j + m - q/2)p - i\pi m}, \quad (9)$$

where $e_j = (j + 1/2)/D$ and K is a normalization factor which converges to $(2/D)^{1/4}$ for $D \gg 1$. The phase has been chosen in such a way that parity and time reversal operators act on them as

$$\hat{R}|q, p\rangle = |1 - q, 1 - p\rangle, \quad (10)$$

$$\hat{T}|q, p\rangle = |p, q\rangle \quad (11)$$

without additional phases.

We now consider the collection of coherent states on the periodic points $|q_i, p_i\rangle$, $i = 0, \ldots, L-1$ of a given primitive orbit labeled by the binary string $\boldsymbol{\nu}$. For chaotic systems the points are isolated and therefore in the semiclassical limit $D \to \infty$ these states are approximately orthogonal. In the same semiclassical limit they satisfy the approximate conditions

$$\langle q_{j+1}, p_{j+1} | q_j, p_j \rangle \simeq \delta_{j+1,j},$$

$$\hat{B}_{j,j+1} \equiv \langle q_{j+1}, p_{j+1} | \hat{B} | q_j, p_j \rangle \simeq \frac{e^{i 2\pi D S_j}}{\sqrt{\cosh \lambda}}, \quad (12)$$

where $q_L \equiv q_0$, $p_L \equiv p_0$; λ is the Lyapunov exponent and where the phase S_j acquired by the coherent state in one step of the map (with the present choice of phases for the coherent states) is

$$S_j \equiv S_{q_j, p_j} = [2q_j]\left(\frac{q_j}{2} + \frac{p_j}{4} + \frac{1}{4} \right). \quad (13)$$

The $L \times L$ matrix $\hat{B}_{j,k}$ in Eq. (12) is cyclic in the semiclassical limit and therefore it can be diagonalized by a discrete Fourier transform. The eigenvalues are given by

$$\langle \phi_{\boldsymbol{\nu}}^k | \hat{B} | \phi_{\boldsymbol{\nu}}^k \rangle \simeq \frac{e^{i 2\pi A_{\boldsymbol{\nu}}^k}}{\sqrt{\cosh \lambda}}, \quad (14)$$

where

$$A_{\boldsymbol{\nu}}^k = \frac{DS_{\boldsymbol{\nu}} + k}{L}. \tag{15}$$

The phase of the eigenvalues involves the classical action of the orbit $S_{\boldsymbol{\nu}} = \Sigma_{j=0}^{L-1} S_j$, and k is a Bohr-Sommerfeld-type parameter which can be chosen from $k = 0, \ldots, L-1$. Each periodic orbit then contributes L complex eigenvalues whose phases are equally spaced and shifted from the origin by $DS_{\boldsymbol{\nu}}/L$.

The eigenfunctions are the periodic orbit modes. They are given explicitly by

$$|\phi_{\boldsymbol{\nu}}^k\rangle = \frac{1}{\sqrt{L}} \sum_{j=0}^{L-1} \exp\left(-i\frac{2\pi(DS_{\boldsymbol{\nu}} + k)j}{L} + i\theta_j\right)|q_j, p_j\rangle, \tag{16}$$

where $\theta_j = 2\pi D \Sigma_{l=0}^{j-1} S_l$. They are labeled by the binary symbol of the periodic orbit and by the discrete index k ($k = 0, \ldots, L-1$). Within the validity of the above approximations they are orthogonal. The fact that the eigenvalues are complex reflects the instability of the orbit and characterizes these states as long-lived resonances whose approximate width on the unit circle is λ. As this width is classical (independent of D) these resonances overlap significantly with a number of eigenstates $\lambda D/2\pi$ which is large in the semiclassical limit.

It is convenient to impose the map symmetries to the POM's. The symmetries of the periodic orbits can be used for this purpose. The PO of the classical baker map can be classified in terms of their invariance under the classical symmetries R and T. We characterize this invariance by two integers σ_R, σ_T with the value $\sigma_R = 0$ or $\sigma_T = 0$ for invariant orbits, while $\sigma_R = 1$ or $\sigma_T = 1$ if there are two different orbits connected by the respective symmetry. As the action $S_{\boldsymbol{\nu}}$ is invariant under these symmetries, the eigenvalues of the POM constructed for each $S_{\boldsymbol{\nu}}$ are degenerate with an associated subspace of dimension $2^{\sigma_T} 2^{\sigma_R}$. In these subspaces it is possible to construct POM's that have the same symmetries as the eigenfunctions. Thus central orbits ($\sigma_R = \sigma_T = 0$) with $\boldsymbol{\nu} = \boldsymbol{\nu}^\dagger = \overline{\boldsymbol{\nu}}$ give rise to L states, which automatically have the required symmetries. Orbits with either $\sigma_R = 0$, $\sigma_T = 1$ or $\sigma_R = 1$, $\sigma_T = 0$ give rise to $2L$ states, while nonsymmetric orbits $\sigma_R = 1$, $\sigma_T = 1$ give rise to $4L$ states. Some examples illustrating this construction are

$$|\tilde{\Phi}_{01}^k\rangle \equiv |\phi_{01}^k\rangle, \tag{17}$$

$$|\tilde{\Phi}_{001}^{k,R=\pm}\rangle \equiv \frac{(1 \pm R)}{\sqrt{2}}|\phi_{001}^k\rangle, \tag{18}$$

$$|\tilde{\Phi}_{001011}^{k,T=\pm}\rangle \equiv \frac{(1 \pm T)}{\sqrt{2}}|\phi_{001011}^k\rangle, \tag{19}$$

$$|\tilde{\Phi}_{0001011}^{k,T=\pm,R=\pm}\rangle \equiv \frac{(1 \pm T)}{\sqrt{2}}\frac{(1 \pm R)}{\sqrt{2}}|\phi_{0001011}^k\rangle, \tag{20}$$

where $k = 0, \ldots, L-1$.

Figure 1 shows the Husimi representation of two symmetrized POM corresponding to $\boldsymbol{\nu} = 001$ and $\boldsymbol{\nu} = 00101$. The bottom part shows the distribution of the squared overlaps with
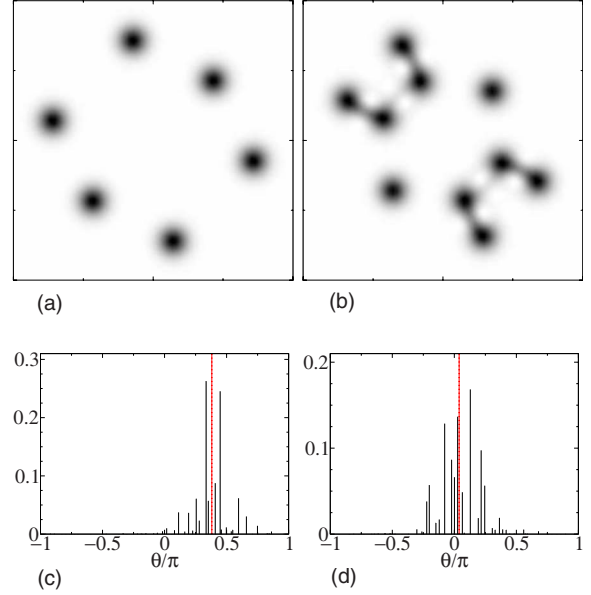

FIG. 1. (Color online) Husimi representation of the periodic orbit modes over 001 $|\tilde{\Phi}_{001}^{1,R=-}\rangle$ (a) and over 00101 $|\tilde{\Phi}_{00101}^{3,R=+}\rangle$ (b) for $D = 120$ in the unit square phase space $q, p \in [0, 1)$. Square modulus of the product of these states $|\langle\psi_j|\tilde{\Phi}_{001}^{1,R=-}\rangle|^2$ (c) and $|\langle\psi_j|\tilde{\Phi}_{00101}^{3,R=+}\rangle|^2$ (d) with eigenstates $|\psi_j\rangle$ with $j = 1, \ldots, D$ ordered by increasing eigenphases. The red dashed line represents the central phase $A_{001}^{k=1}$ and $A_{00101}^{k=3}$.

the eigenstates as a function of the eigenphases. The central dotted line is the Bohr-Sommerfeld energy in Eq. (15). It should be clear that this construction can be justified for a fixed periodic orbit, and for $D \to \infty$ because the periodic points of chaotic systems are isolated. However, if we want these quasimodes as a basis for a fixed value of D we need also to consider orbits where the assumptions in Eq. (12) are not satisfied. Instead of a diagonalization by means of an explicit Fourier transform we must consider the generalized eigenvalue problem $\det[\langle q_i, p_i|\hat{B}|q_j, p_j\rangle - \lambda\langle q_i, p_i|q_j, p_j\rangle] = 0$. We explore this problem in connection to homoclinic orbits in the Appendix.

B. Scar functions

In the preceding section we have seen that the POM are quasienergy wave packets of constant classical width λ. Narrower wave packets can be constructed by Fourier transforming the POM's evolved for a limited time [7–11,13]. The resulting states are the scar functions.

Consider the following operator which depends on the time parameter t and the phase ε

$$\hat{P}_t(\varepsilon) = \sum_{l=-\infty}^{\infty} e^{-i\varepsilon l} e^{-l^2/2t^2} \hat{B}^l. \tag{21}$$

When the Gaussian window is allowed to have infinite width ($t \to \infty$), this operator projects on the quasienergy eigenstates while for finite t the corresponding width will be $\Delta\varepsilon = 2\pi/t$. In general, we have
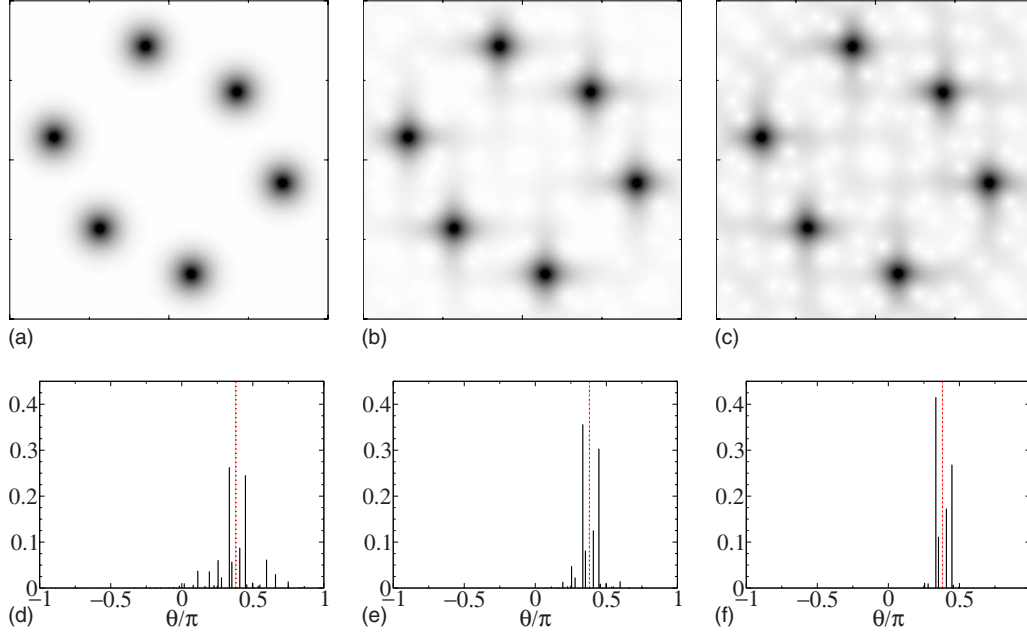
FIG. 2. (Color online) Husimi representation of the scar functions, in the unit square phase space ($q, p \in [0, 1)$), over $\boldsymbol{\nu} = 001$ with different propagation times $|\Phi_{001}^{t=0,k=1,R=-}\rangle$ ($t=0$) (a), $|\Phi_{001}^{t=2,k=1,R=-}\rangle$ ($t=2$) (b), and $|\Phi_{001}^{t=4,k=1,R=-}\rangle$ ($t=4$) (c) for $D=120$. We plot the square root of the Husimi function to enhance the structure on the manifolds. Square modulus of the product of these states $|\langle\psi_j|\Phi_{001}^{t,k=1,R=-}\rangle|^2$ for $t=0$ (d), $t=2$ (e), $t=4$ (f) with eigenstates $|\psi_j\rangle$ with $j=1,\dots,D$ ordered by increasing eigenphases. The red dashed line represents the central phase $A_{001}^{k=0}$.

$$\hat{P}_t(\varepsilon) = \sum_{j=1}^{D} \sum_{l=-\infty}^{\infty} e^{-i\varepsilon l} e^{-l^2/2t^2} \langle\psi_j|\hat{B}^l|\psi_j\rangle |\psi_j\rangle\langle\psi_j|$$

$$= \sum_{j=1}^{D} \delta_t(\varepsilon - \varphi_j) |\psi_j\rangle\langle\psi_j|, \tag{22}$$

where $\delta_t(\varepsilon)$ is the Fourier transform of $e^{-l^2/2t^2}$. When this operator acts on a POM it sharpens its quasienergy width while extending the wave packet in phase space along the stable and unstable manifolds of the periodic orbit. A wave function is thus created that interpolates between a simply constructed but relatively unstable state and a true eigenstate if the propagation time is of the order of the Heisenberg time. The interesting region is of course when the propagation time is of the order of the Ehrenfest time. We define the scar functions as the short-time propagation ($\propto$ Ehrenfest time $= \log_2 D$) of POM in $\boldsymbol{\nu}$ with the phase evaluated in $\varepsilon = A_{\boldsymbol{\nu}}^k$ defined by Eq. (15),

$$|\Phi_{\boldsymbol{\nu}}^{t,k}\rangle \equiv \frac{1}{\kappa} \hat{P}_t(2\pi A_{\boldsymbol{\nu}}^k) |\tilde{\Phi}_{\boldsymbol{\nu}}^k\rangle, \tag{23}$$

where κ is a normalization factor, and the POM is recovered for $t=0$ ($|\Phi_{\boldsymbol{\nu}}^{t=0,k}\rangle \equiv |\tilde{\Phi}_{\boldsymbol{\nu}}^k\rangle$). Notice that, for unstable periodic orbits, the forward and backward propagation of wave packets on the periodic points lead to significant amplitude on the stable and unstable manifolds of that orbit. It is then expected [10,11] that these scar functions will be structures supported on these manifolds and having narrower overlaps with definite quasienergy regions on the unit circle. In this

work we fix the phase ε to the Bohr-Sommerfeld values ($A_{\boldsymbol{\nu}}^k$) and vary the time propagation t.

The Husimi representations of the scar functions over $\boldsymbol{\nu} = 001$ for different evolution times ($t=0,2,4$), and their products with QBM eigenstates are shown in Fig. 2. Note that the coherent states in the Husimi representation spread in the stable and unstable manifolds interfering between each other. Note that the Ehrenfest time for $D=120$ is approximately $t_{\text{Ehr}} \sim 7$.

TABLE I. Periodic orbits used in basis construction of dimension D_s to describe the QBM spectrum of dimension D (where $D_s \geq D$).

| Dimension		Periodic orbit added
D_s	$L_{\boldsymbol{\nu}}$	$\boldsymbol{\nu}$
2	1	0
4	2	01
10	3	001
22	4	0001; 0011
52	5	00001; 00011; 00101
106	6	000001; 000011; 000101; 000111; 001011
232	7	0000001; 0000011; 0000101; 0001001;
		0000111; 0001011; 0001101; 0010011; 0010101
472	8	00000001; 00000011; 00000101; 00001001;
		00000111; 00001011; 00001101; 00010101;
		00011001; 00010011; 00100101; 00001111;
		00010111; 00011011; 00101011; 00101101
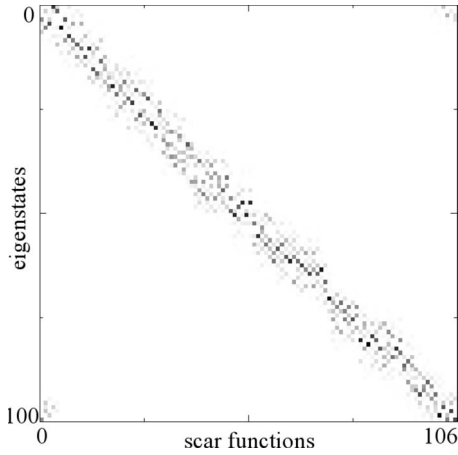
FIG. 3. Overlap matrix, $|\langle\psi_j|\Phi_\nu^{t,k,R,T}\rangle|^2$, between the eigenstates of the QBM ordered by eigenphases and the scar functions constructed on the PO with $L \leq 6$, ordered by increasing phase A_ν^k for $D=100$ ($|\psi_j\rangle$ on rows and $|\Phi_\nu^{t=t_{Ehr}/2,k,R,T}\rangle$ on columns). The value of the overlap is in grayscale from 0 (white) to 1 (black).

IV. NUMERICAL TEST OF THE BASIS

Scar function basis. The QBM can be simplified using the scar functions as basis. In fact, it is useful to choose a set of D_S nonorthogonal scar functions, which span the D-dimensional Hilbert space, as an overcomplete basis of the QBM. The election of the periodic orbits will determine the basis. As we want to construct functions on short PO we give two different rules to choose the PO of the basis which converge to the same basis for long D.

(1) The first choice is to select the PO with the shortest period which spans the Hilbert space. For example, for $D=100$ we will have $D_S=106$ scar functions constructed over PO with period up to $L=6$, and for $D=140$ we must include PO with period $L=7$ and therefore $D_S=232$ (see Table I for $D \leq 472$).

(2) The other possible election of the PO could be, for a given D, to choose $D_S=2^L \in [D, 2D)$ and the short PO labeled by binary strings of L digits.

In this work we will choose the shortest period basis, but for long D limit both bases, are similar. The important fact is that in both cases the maximum period involved grows as $\log_2 D$. Figure 3 shows the overlap matrix $|\langle\psi_j|\Phi_\nu^{t,k,R,T}\rangle|^2$ of QBM eigenstates ($D=100$) ordered by eigenphases ($|\psi_j\rangle$, on rows) and the scar function basis ($D_S=106$) ($|\Phi_\nu^{t=t_{Ehr}/2,k,R,T}\rangle$, on columns) ordered by phase value A_ν^k, with $t=t_{Ehr}/2$.

This result, besides restating the fact that scar functions have narrow overlaps with eigenstates also shows that an eigenstate can be pictured as a narrow superposition of scars. Each of which is relatively simple to construct. For example, in the case of $D=102$ one of the eigenstates of the QBM can be represented by only one scar function of period $L=3$ with a propagation time of $t=t_{Ehr}/2$ with an accuracy of $|\langle\psi_j|\Phi_{001}^{t_{Ehr}/2,k=2,R=+}\rangle| \simeq 0.87$. The approximation of the eigenstate can be improved adding another scar function of period $L=4$. Therefore, an ansatz state constructed as

$$|\Phi_{ansatz}\rangle = c_1|\Phi_{001}^{t_{Ehr}/2,k=2,R=+}\rangle + c_2|\Phi_{0001}^{t_{Ehr}/2,k=2,R=+}\rangle \quad (24)$$

with $c_1 \simeq 0.75$ and $c_2 \simeq 0.48e^{-i0.117}$ has an accuracy of $|\langle\psi_j|\Phi_{ansatz}\rangle| \simeq 0.92$. Figure 4 shows the Husimi functions of the eigenstates and both scar functions considered in this example.

The scar functions have superposition with a small number of eigenstates. This can be quantified in terms of the average participation ratio defined as

$$\langle PR \rangle = \frac{1}{D_S} \sum_{L=l} \left(\sum_{j=1}^{D} |\langle\psi_j|\Phi_\nu^{t,k,R,T}\rangle|^4 \right)^{-1}, \quad (25)$$

where $\langle PR \rangle \in [1, D)$. Notice that the random matrix theory prediction for a generic basis is $\langle PR \rangle = D/2$.

The $\langle PR \rangle$ decreases with the propagation time and converges to 1 in the Heisenberg time limit as was expected. However, the interesting region is for times of the order of the Ehrenfest time. In Fig. 5(a) we show $\langle PR \rangle$ as a function of propagation time for $D=34, 66, 130$. In Fig. 5(b) we also show the fraction of scar functions which have PR less than 1.5 as a function of time. Notice that for $D=130$ and at $t \simeq t_{Ehr}$ the average number of eigenstates in a scar is about three and 20% of the scar states have a $\langle PR \rangle$ less than 1.5 meaning that they are almost pure eigenstates.

The average participation ratio as a function of the dimension of the QBM is shown in Fig. 6 for the POM and the scar functions with $t=t_{Ehr}/2$ and $t=t_{Ehr}$. For the limited range of values available the $\langle PR \rangle$ seems to grow linearly with D but with a slope significantly smaller than the $D/2$ random matrix value. The reduction is similar (and more important) than that obtained in [1,2].
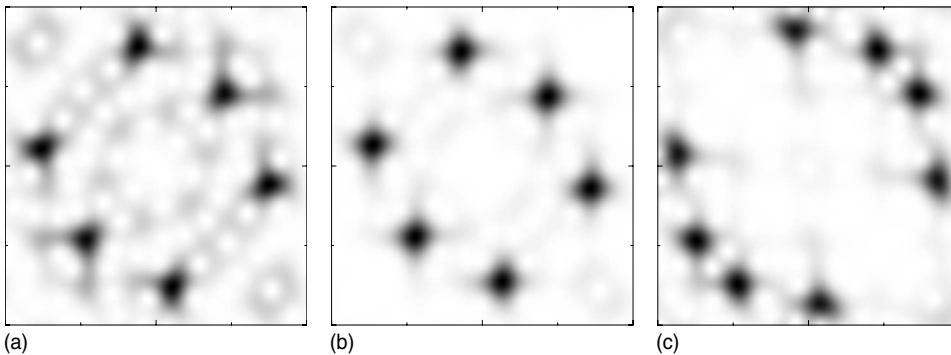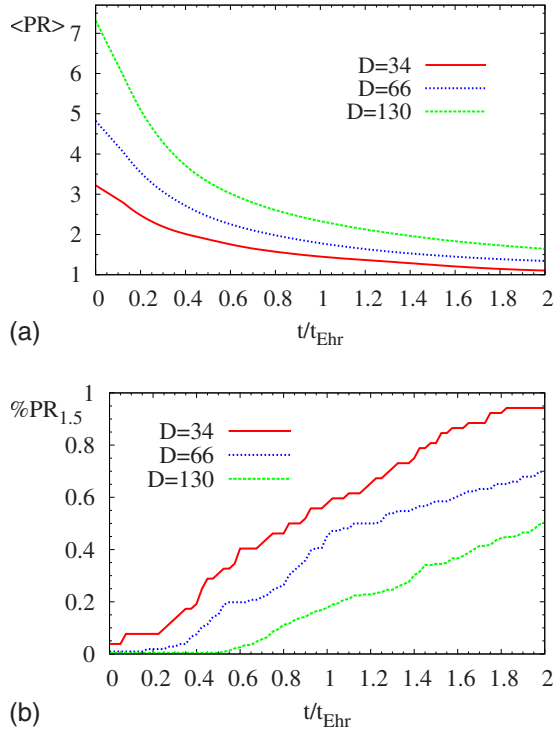

(a)　　　　(b)　　　　(c)

FIG. 4. Husimi representation in the unit square phase space ($q, p \in [0,1)$) of an eigenstate of the QBM for $D=102$ (a), and its most prominent scar function components (b,c) as given in Eq. (24).

FIG. 5. (Color online) (a) Average participation ratio ($\langle PR \rangle$) as a function of the propagation time for $D = 34, 66, 130$ in units of Ehrenfest time. (b)$\% PR_{1.5}$, fraction of scar functions which have $PR < 1.5$ in the QBM eigenstates basis.

V. SCAR APPROXIMATION BY HOMOCLINIC PERIODIC ORBIT MODES

The construction of the POM basis is a simple analytical formula only involving as classical input short periodic orbits. The scar function requires in addition the forward and backwards propagation of the POM. In this paper for simplicity this propagation was obtained exactly by a matrix multiplication. It should be clear, however, that accurate semiclassical expressions for this propagation could be available as long as the times involved remain bounded by the Ehrenfest time. In this section we illustrate a different approach that replaces the need for this propagation by the
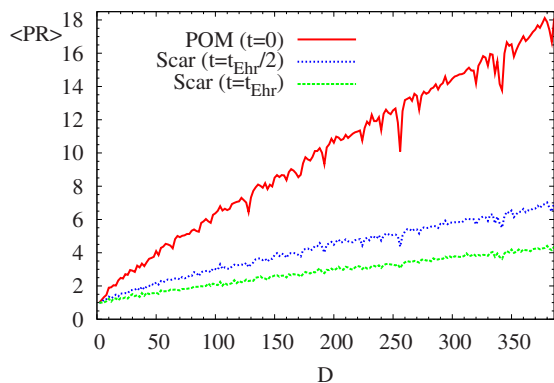

FIG. 6. (Color online) Average participation ratio ($\langle PR \rangle$) as a function of the dimension of the QBM for the POM and the scar functions with $t = t_{Ehr}/2$ and $t = t_{Ehr}$.
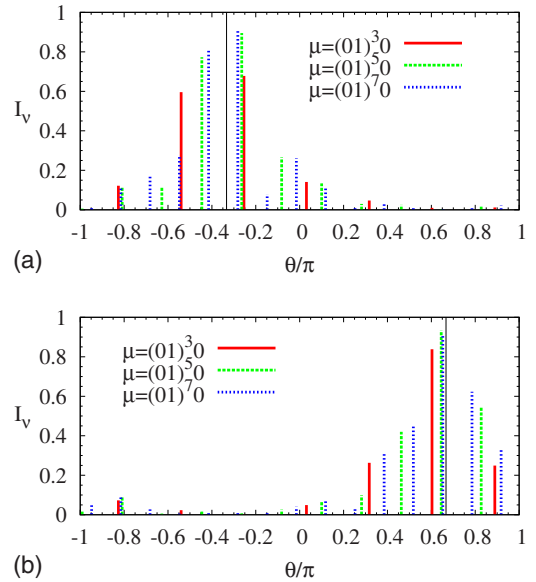

FIG. 7. (Color online) Intensity $I_\nu \equiv |\langle \Phi_\nu^{t_{Ehr}/2, k_\nu} | \Phi_\mu^{0, k_\mu} \rangle|$ between the scar function over $\nu = 01$ with $t = t_{Ehr}/2$, and the homoclinic POM over $\mu = (01)^s 0$ with $s = 3, 5, 7$. $k_\nu = 0$ is shown in (a) and $k_\nu = 1$ in (b), where respective phases are drawn with solid black lines. The dimension of the Hilbert space is $D = 128$ and the products are ordered by increasing phase (θ) of μ for the $2s + 1$ values of k_μ.

construction of POM's on long periodic orbits homoclinic to short ones.

The homoclinic POM are simply the POM construction described in Sec. III A over PO of the form $\mu = (\nu)^s h$ with period $L_\mu = s L_\nu + L_h$. This PO resembles the homoclinic trajectories of ν with the excursion h represented by the infinite string $\cdots \nu\nu\nu h \nu\nu\nu \cdots$, and converges to it in the long s limit. These orbits for large s accumulate near stable and unstable manifolds of ν and therefore can mimic the building up of amplitude produced by the propagation.

A long POM with period L_μ will generate L_μ states with phases $A_\mu^{k_\mu}$ uniformly spaced on the unit circle. The state with the phase $A_\mu^{k_\mu}$ closer to $A_\nu^{k_\nu}$ of the short ν orbit will have the largest overlap with the scar state. An example is shown in Fig. 7 for the product between the scar function on $\nu = 01$ for both values of k_ν ($k = 0$ on the left-hand side and $k = 1$ on the right-hand side) with $t = t_{Ehr}$ and the homoclinic POM over $\mu_s = (\nu)^s h$ for all values of k_μ ($I_\nu \equiv |\langle \Phi_\nu^{t_{Ehr}, k_\nu} | \Phi_\mu^{t = 0, k_\mu} \rangle|$) as a function of the phase which takes the discrete value A_μ^k. In this case we choose the shortest homoclinic excursion $h = 0$ and values of $s = 3, 5, 7$. In this example acceptable approximations ($I_\nu \gtrsim 0.9$) are reached for values of s no longer than 7. In Fig. 8 we compare the Husimi representations of the scar function on $\nu = 01$ with $k = 1$ and $t = t_{Ehr}/2$ and its best approximation with the homoclinic POM over $\mu_s = (01)^s 0$ with $s = 7$. Note that the homoclinic POM structure looks similar to the evolution in time of the scar since it spreads the stable and unstable manifolds of the PO.

VI. CONCLUSIONS

We have shown that a set of states constructed on the periodic orbits of the QBM provides a way of describing its
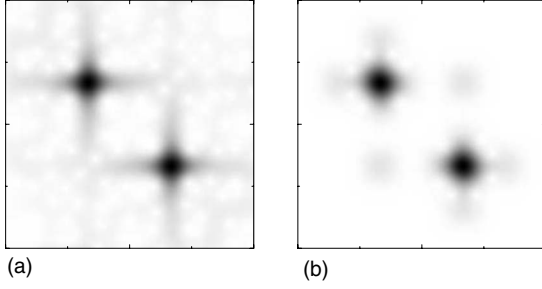
(a)   (b)

FIG. 8. (a) Husimi representation in the unit square phase space of the scar function $|\Phi_\nu^{t_{\mathrm{Ehr}}/2,k=1}\rangle$ on the PO $\nu=01$. (b) The Husimi representation of the POM $|\Phi_\mu^{0,k=12}\rangle$ constructed on the homoclinic orbit $\mu=(01)^s 0$ (with $s=7$) which approximates the scar function. We plot the square root of the Husimi function to enhance the structure on the manifolds. Those states are the scar function and the POM approximation of the scar of Fig. 7, respectively, for $D=128$.

eigenfunctions which significantly improves (in terms of the average participation ratio) the description in terms of a generic basis. For the QBM this improvement is similar to that obtained by Lakshminarayan using the Hadamard basis [1] or by the essential baker map [2]. However, the method does not use any special structure of the chaotic map and should be generally applicable to other chaotic maps [21] as long as the properties of a limited set of periodic orbits are known.

The construction is still far from a full semiclassical analysis. The basis that we constructed is nonorthogonal and requires us to consider each primitive orbit as noninteracting with each other periodic orbit. The semiclassical calculation of this interaction would be needed to calculate the amplitudes that describe the eigenstates in terms of scar states. Calculation of this type has been performed for the billiard stadium [10,11,22], an hyperbolic Hamiltonian [23], and linear maps on the torus ("cat maps") [21].

It is also important to mention that the aim here is to reconstruct the unitary dynamics of the map in terms of pure states constructed as interpretations of Gaussian packets with complex coefficients derived from the classical action. A different construction based on incoherent superposition of densities placed on periodic points would allow for a similar reconstruction in terms of the Liouville dynamics. We postpone this aspect of the problem for future investigations.

ACKNOWLEDGMENTS

APPENDIX: POM DIAGONALIZATION

The periodic orbit modes (POM) constructed in Sec. III A can also be seen in a different light. Consider the generalized eigenvalue problem

$$\det(\langle \gamma_i | \hat{B} | \gamma_j \rangle - z \langle \gamma_i | \gamma_j \rangle) = 0, \tag{A1}$$
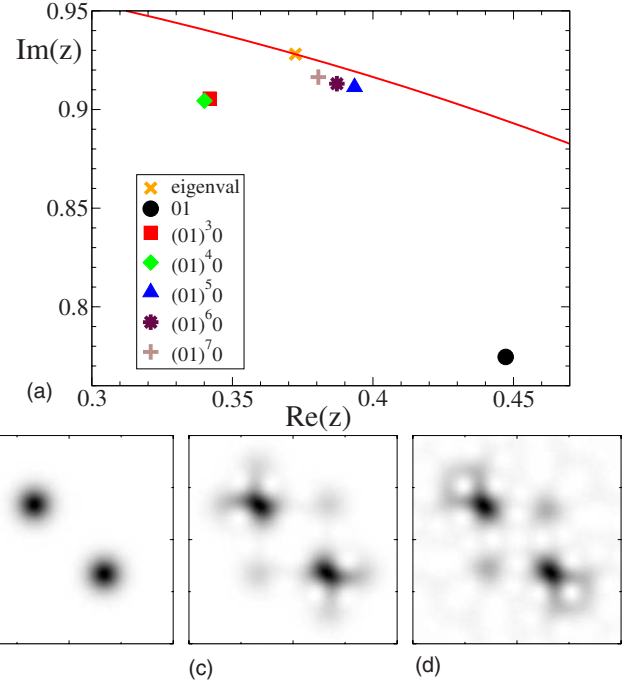

(a)

(b)   (c)   (d)

FIG. 9. (Color online) (a) Real and imaginary part of the solutions of the generalized eigenvalue problem for the PO $\nu=01$ and the homoclinic orbit family $\mu=(01)^s 0$ for $s=3,4,5,6,7$. with $D=50$. These solutions converge to the exact eigenvalue which lives in the unit circle (solid line). Bottom: Husimi functions in the unit square phase space of the states associated with the eigenvalues marked with $\bullet$ ($\mu=01$), $+$ [$\mu=(01)^7 0$], and $\times$ (the exact eigenstate of the map) [(b,c,d), respectively.

where $|\gamma_i\rangle$ are coherent states placed on M periodic points of the map. The operator $\Sigma_i^M |\gamma_i\rangle\langle\gamma_i|$ can be considered as an approximation to the resolution of unity in the D-dimensional Hilbert space, characteristic of coherent states as long as M is large enough ($\gtrsim D$) and the points cover uniformly the phase space. This latter condition is satisfied for chaotic maps on account of the Hannay–Ozorio de Almeida sum rule [24]. Under this condition Eq. (A1) provides D exact eigenvalues and M-D zero eigenvalues [25].

POM are obtained with the two assumptions:

(a) Different primitive orbits do not interact.

(b) Equation (12) is satisfied.

With these conditions the eigenvalue problem is solved by a simple Fourier transform involving the different points on an orbit. The eigenfunctions are the POM's of Eq. (16) and the eigenvalues are complex and given by Eq. (14).

If we only retain the assumption that periodic orbits do not interact we can refine the construction of POM by considering the limited diagonalization [Eq. (A1)] where now $|\gamma_i\rangle$ are the points on a primitive orbit (and its image under R and T if necessary). This refinement is important for long orbits of the type $\mu=\nu^s h$ and $\mu=\nu_1^{s_1} h \nu_2^{s_2}$ which mimic homoclinic and heteroclinic orbits and accumulate their points close to short primitive orbits. For these orbits it is not correct to assume the coherent states as being even approximately orthogonal and therefore the generalized diagonaliza-

tion is necessary. The eigenvalues divide in two sets. Some converge rapidly to very small values, while there are always some of them which converge to the unit circle.

The advantage of this construction is that the "good" eigenvalues are closer to the unit circle and therefore represent modes that have a longer lifetime. Moreover, spurious eigenvalues that are produced by the superposition of many almost equal coherent states are rapidly eliminated. The disadvantage is of course that the construction is not analytic and requires a diagonalization.

We give an example for the family of orbits $\boldsymbol{\mu}_s = \boldsymbol{\nu}^s \mathbf{h}$. We have diagonalized Eq. (A1) for periodic points on the orbit $\boldsymbol{\mu}_s$ ($s = 3, 4, 5, 6, 7$) and compare with the exact eigenstate of the QBM for $D = 50$ (Fig. 9).

[1] A. Lakshminarayan and N. Meenakshisundaram, J. Phys. A **39**, 11205 (2006); A. Lakshminarayan, *ibid.* **38**, L597 (2005).

[2] L. Ermann and M. Saraceno, Phys. Rev. E **74**, 046205 (2006).

[3] H Poincaré, *Les Méthodes Nouvelles de la Mecánique Céleste* (Guathier-Villars, Paris, 1892), Vol. I, Chap. III, article 36, as quoted by M. Barenger in M. Baranger, M. R. Haggerty, B. Lauritzen, D. C. Meredith, and D. Provost, Chaos **5**, 261 (1995).

[4] E. J. Heller, Phys. Rev. Lett. **53**, 1515 (1984); L. Kaplan and E. Heller, Ann. Phys. (N.Y.) **264**, 171 (1998).

[5] M. V. Berry, in *Chaotic Behavior in Deterministic Systems*, edited by G. Iooss, R. Hellemann, and R. Stora (North-Holland, Amsterdam, 1983), p. 171.

[6] A. J. Schnirelman, Usp. Mat. Nauk **29**, 181 (1974); Y. Colin de Verdiere, Commun. Math. Phys. **102**, 497 (1985).

[7] L. Kaplan, Phys. Rev. Lett. **80**, 2582 (1998).

[8] L. Kaplan and E. J. Heller, Phys. Rev. E **59**, 6609 (1999); L. Kaplan, Nonlinearity **12**, R1 (1999).

[9] W. E. Bies, L. Kaplan, M. R. Haggerty, and E. J. Heller, Phys. Rev. E **63**, 066214 (2001).

[10] E. Vergini, J. Phys. A **33**, 4709 (2000).

[11] E. Vergini and G. Carlo, J. Phys. A **33**, 4717 (2000).

[12] S. Y. Lee and S. C. Creagh, Ann. Phys. **307**, 392 (2003).

[13] F. Faure, S. Nonnenmacher, and S. De Bievre, Commun. Math. Phys. **239**, 449 (2003).

[14] D. A. Wisniacki, F. Borondo, E. Vergini, and R. M. Benito, Phys. Rev. E **63**, 066220 (2001).

[15] V. I. Arnold and A. Alvez, *Ergodic Problems of Classical Mechanics* (Benjamin, New York, 1968).

[16] N. L. Balazs and A. Voros, Ann. Phys. **190**, 1 (1989).

[17] M. Saraceno, Ann. Phys. **199**, 37 (1990).

[18] M. Saraceno and A. Voros, Physica D **79**, 206 (1994).

[19] F. P. Simonotti, E. Vergini, and M. Saraceno, Phys. Rev. E **56**, 3859 (1997).

[20] P. Leboeuf and A. Voros, J. Phys. A **23**, 1765 (1990); S. J. Chang and K. J. Shi, Phys. Rev. Lett. **55**, 269 (1993).

[21] E. G. Vergini, D. Schneider, and A. M. F. Rivas, J. Phys. A: Math. Theor. **41**, 405102 (2008).

[22] E. G. Vergini and G. G. Carlo, J. Phys. A **34**, 4525 (2001).

[23] E. G. Vergini and D. Schneider, J. Phys. A **38**, 587 (2005).

[24] J. H. Hannay and A. M. Ozorio de Almeida, J. Phys. A **17**, 3429 (1984).

[25] P. Gerwinski, F. Haake, H. Wiedemann, M. Kus, and K. Zyczkowski, Phys. Rev. Lett. **74**, 1562 (1995).